decreasing growth in the early limb bud, such as inhibition of the growth of blood vessels[9], could also contribute later to decreased growth of the skeletal elements, leading to shortening of the long bones. Although this is not strictly a patterning defect, it is commonly observed in thalidomide cases.

Finally, after the period of exposure to thalidomide, the progress zone would recover, leading to the range of patterning defects occasionally seen, including amelia (absence of limbs), phocomelia, and radial aplasia (lack of development of the radius). The limb patterning defects of thalidomide are therefore the understandable and expected result of decoupling distalization from outgrowth during limb pattertning.

Clifford J. Tabin
Department of Genetics,
Harvard Medical School,
200 Longwood Avenue,
Boston, Massachusetts 02115, USA
e-mail: tabin@rascal.med.harvard.edu

1. Lenz, W. *Lancet* **1,** 45 (1962).
2. Toms, D. A. Lancet **4,** 400 (1962).
3. Stephens, T. D. *Teratology* **38,** 229–239 (1988).
4. Saunders, J. W. Jr *J. Exp. Zool.* **108,** 363–404 (1948).
5. Summerbell, D. & Lewis, J. H. *J. Embryol. Exp. Morphol.* **33,** 621–643 (1975).
6. Niswander, L., Tickle, C., Vogel, A., Booth, I. & Martin, G. R. *Cell* **75,** 579–587 (1993).
7. Fallon, J. F. *et al. Science* **264,** 104–107 (1994).
8. Wolpert, L., Tickle, C. & Sampford, M. *J. Embryol. Exp. Morphol.* **50,** 175–198 (1979).
9. Kenyon, B. M., Browne, F. & D'Amato, R. J. *Exp. Eye Res.* **64,** 971–978 (1997).

Mistakes not necessary for Müllerian mimicry

In a recent News and Views article[1], Ruxton showed with admirable clarity how the ingenious simulations by MacDougall and Stamp Dawkins[2] of defensive mimicry in animals highlight the role of cognitive limitations of predators in the generation of relationships involving mimicry. However, Ruxton misrepresents my work[3], on which MacDougall and Stamp Dawkins have drawn, thereby giving a misleading impression that mistakes in prey recognition by predators are necessary for the generation of Müllerian mimicry. In fact, the 'virtual predator' on which MacDougall and Stamp Dawkins and others[4] base their work quite ably generates Müllerian mimicry without depending on predator discrimination errors.

Michael P. Speed
Environmental and Biological Studies,
Liverpool Hope University College,
Hope Park, Liverpool L16 9JD, UK

1. Ruxton, G. D. *Nature* **394,** 833–834 (1998).
2. MacDougall, A. & Stamp Dawkins, M. *Anim. Behav.* **55,** 1281–1288 (1988).
3. Speed, M. P. *Anim. Behav.* **45,** 571–580 (1993).
4. Owen, R. E. & Owen, A. R. G. *J. Theor. Biol.* **109,** 217–247 (1984).

Encapsulated C_{60} in carbon nanotubes

Pulsed laser vaporization of graphite in the presence of certain metallic catalysts produces both carbon nanotubes and C_{60} molecules[1]. In nanotube production, most of the C_{60} is removed, along with other residual contaminants, by purification and annealing. It has been suggested that C_{60} may be trapped inside a nanotube during this elaborate sequence, but this has not been detected.

Here we use high-resolution transmission electron microscopy (HRTEM) to show that closed carbon shells are contained within appropriately sized, single-walled nanotubes. Measurements of the diameter of these endofullerenes suggest that many of them are C_{60} molecules. Some of them are observed as self-assembled chains with nearly uniform centre-to-centre distances and resemble a nanoscopic peapod. The endofullerenes coalesce into longer capsules under the action of the electron beam.

HRTEM observations were made on purified nanotube material that had been synthesized by pulsed laser vaporization (from A. G. Rinzler and R. E. Smalley). An HRTEM image of an isolated single-walled nanotube is shown in Fig. 1. The image is dark where the electrons encounter the most carbon atoms and are maximally scattered. The parallel lines are the images of opposing tubule walls that are at a tangent, or nearly so, to the electron beam. The lines are separated by between 1.3 and 1.4 nanometres, which is consistent, within the resolution of the microscope, with the diameter of a typical nanotube. Between the lines are ten collinear circles approximately 0.7 nanometres in diameter and spaced 0.3 nanometres from the tubule walls.

These are the expected measurements for C_{60} contained within the tube and separated from it by a graphitic Van der Waals gap[2]. Furthermore, contrast from the circles is similar to that from the tubule walls, so the constituent atoms are probably carbon

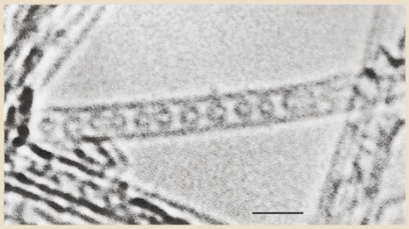

Figure 1 A single-walled carbon nanotube containing a row of closed carbon shells concentric with the tubule axis. The diameter and centre-to-centre spacing of the internal shells are consistent with a chain of C_{60} molecules. The nanotube is surrounded by a vacuum. Scale bar, 2.0 nanometres.

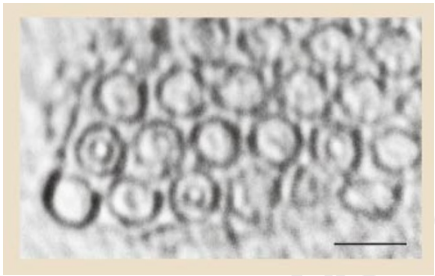

Figure 2 Cross-sectional image of a rope comprising hexagonally packed parallel single-walled carbon nanotubes. At least three tubes contain concentric circular features that are consistent with C_{60}-sized fullerenes. Scale bar, 2.0 nanometres.

rather than a heavier element. Most circles are 1.0 nanometre apart, centre-to-centre, which is the nearest-neighbour spacing in face-centred-cubic C_{60} (ref. 3), but this separation is slightly less for two pairs.

The HRTEM image shown in Fig. 2 also indicates the presence of contained fullerenes. It shows the cross-section of a rope of single-walled nanotubes that is curved such that the tubule axes are approximately parallel to the electron beam. The image of each tubule is a dark circle 1.3 to 1.4 nanometres in diameter. The tubules are packed hexagonally and are separated by approximately 0.3 nanometres, the expected Van der Waals spacing of tubes in a rope. Three tubes that clearly have an inner concentric circle are interspersed in the lattice. These inner circles cannot be Fresnel artefacts because adjacent tubes in the same focus condition show no internal contrast. The inner circles are about 0.7 nanometres in diameter and are interpreted as the images of contained fullerenes the size of C_{60} molecules.

After extended exposure to a 100-kilovolt electron beam, the endofullerenes were sometimes seen to coalesce into longer capsules that were oblong, with C_{60}-like caps at the ends. The long parallel walls maintained a nearly uniform spacing of 0.3 nanometres from the walls of the outer tube. Lengths corresponding to the coalescence of three or four spherical molecules were seen. This behaviour may be understood by considering that the energy of binding of a carbon atom to a C_{60} 'buckyball' is about 0.6 electronvolts less than to a nanotube[4]. For an electron beam of a given energy, this difference means that that a carbon atom is more likely to be displaced from C_{60} than from a nanotube. The coalescence may therefore be the reconfiguration of damaged C_{60} into more stable capsule structures, with the dimensions constrained by the surrounding nanotube.

Most nanotubes do not contain fullerenes, although many such assemblies were seen. Stable, closed, carbon shells exist inside single-walled carbon nanotubes, and there is strong evidence that many of these

endofullerenes are self-assembled chains of C_{60}. The observation of these structures raises the hope that refined processing techniques can be developed to produce them in large quantities.

Brian W. Smith*, Marc Monthioux*†, David E. Luzzi*

**Department of Materials Science and Engineering, University of Pennsylvania, 3231 Walnut Street, Philadelphia, Pennsylvania 19104-6272, USA*
e-mail: luzzi@lrsm.upenn.edu
†CEMES, UPR A-8011 CNRS, BP 4347, F-31055 Toulouse cedex 4, France

1. Rinzler, A. G. *et al. Appl. Phys. A* **67,** 29–37 (1998).
2. Nikolaev, P., Thess, A., Rinzler, A. G., Colbert, D. T. & Smalley, R. E. *Chem. Phys. Lett.* **266,** 422–426 (1997).
3. Heiney, P. A. *J. Phys. Chem. Solids* **53,** 1333–1352 (1992).
4. Yakobson, B. I. & Smalley, R. E. *Am. Sci.* **85,** 324–337 (1997).

How does xenon produce anaesthesia?

Since the discovery that the gas xenon can produce general anaesthesia[1] without causing undesirable side effects, we have remained surprisingly ignorant of the molecular mechanisms underlying this clinical activity of an 'inert' gas. Although most general anaesthetics enhance the activity of inhibitory $GABA_A$ (γ-aminobutyric acid type-A) receptors[2,3], we find that the effects of xenon on these receptors are negligible. Instead, xenon potently inhibits the excitatory NMDA (*N*-methyl-D-aspartate) receptor channels, which may account for many of xenon's attractive pharmacological properties.

We found that xenon had virtually no effect on $GABA_A$ receptors. Currents activated by 3 μM GABA, both in voltage-clamped cultured rat hippocampal neurons and in voltage-clamped PA3 cells[4] that stably expressed defined $GABA_A$ subunits, were not significantly affected even by 100% xenon (to function as a human anaesthetic, the half-maximal effective concentration (EC_{50}) is 71% v/v; ref. 5). Xenon also had little effect on functional GABA-releasing synapses in hippocampal neurons, with 80% xenon reducing peak inhibitory postsynaptic currents by only 8 ± 2%. This result indicates that the presynaptic effects of xenon must also be very modest.

Apart from the $GABA_A$ receptor, the only generally accepted neuronal target of conventional anaesthetics is the NMDA receptor. This subtype of glutamate-activated ionotropic channels is implicated in synaptic mechanisms underlying learning, memory and the perception of pain[6]. The NMDA receptor is also believed to be a target of the intravenous general anaesthetic agent ketamine[7], and possibly nitrous oxide[8].

We therefore looked at the effects of xenon on NMDA-activated currents in cultured hippocampal neurons. We found that 80% xenon, which will maintain surgical anaesthesia, reduced NMDA-activated currents by about 60% (Fig. 1a), with no significant change in the NMDA EC_{50} value or Hill coefficient. This non-competitive inhibition indicates that xenon should strongly inhibit neural transmission, despite the high glutamate concentrations in synaptic clefts.

We then tested this in microisland cultures of hippocampal neurons that form synapses with themselves (autapses)[9]. A typical glutamatergic postsynaptic current recorded from a hippocampal neuron is shown in Fig. 1b. The control records show a characteristic biphasic time course, with a fast component mediated by non-NMDA receptors and a much slower component mediated by NMDA receptors. This NMDA receptor-mediated component could be readily identified as it was blocked by the highly selective competitive antagonist AP5 (DL-2-amino-5-phosphonopentanoate)[10].

Addition of 200 μM AP5 almost completely blocked the slow component, leaving only a fast component, with a single exponential time course very similar to that of the control fast component. The effect of xenon on the glutamatergic postsynaptic current resembled that of AP5 (Fig. 1b). The slow, NMDA-receptor-mediated component was reduced by over 70%, whereas the fast component barely changed. So, not only did xenon inhibit synaptic NMDA receptors, it had little apparent effect on non-NMDA receptors.

If xenon exerts its effects by inhibiting NMDA receptors, then this explains some important features of its pharmacological profile, particularly as NMDA-receptor antagonists can relieve pain and cause amnesia, which are features of xenon anaesthesia. Like nitrous oxide ('laughing gas'), which may also act, at least partly, on NMDA receptors[8], xenon can induce a state of euphoria. Other neuronal targets for xenon may emerge, but its powerful inhibition of the NMDA receptor is likely to be instrumental in the anaesthetic and analgesic effects of this 'inert' gas.

N. P. Franks, R. Dickinson, S. L. M. de Sousa, A. C. Hall, W. R. Lieb

Biophysics Section, The Blackett Laboratory, Imperial College of Science, Technology and Medicine, Prince Consort Road, London SW7 2BZ, UK
e-mail: n.franks@ic.ac.uk

1. Cullen, S. C. & Gross, E. G. *Science* **113,** 580–582 (1951).
2. Franks, N. P. & Lieb, W. R. *Nature* **367,** 607–614 (1994).
3. Mihic, S. J. *et al. Nature* **389,** 385–389 (1997).
4. Hadingham, K. L. *et al. Proc. Natl Acad. Sci. USA* **89,** 6378–6382 (1992).
5. Cullen, S. C., Eger, E. I. II, Cullen, B. F. & Gregory, P. *Anesthesiology* **31,** 305–309 (1969).
6. Rang, H. P., Dale, M. M. & Ritter, J. M. *Pharmacology* 3rd edn (Churchill Livingstone, Edinburgh, 1995).
7. Anis, N. A., Berry, S. C., Burton, N. R. & Lodge, D. *Br. J. Pharmacol.* **79,** 565–575 (1983).
8. Jevtovic-Todorovic, V. *et al. Nature Med.* **4,** 460–464 (1998).
9. Bekkers, J. M. & Stevens, C. F. *Proc. Natl Acad. Sci. USA* **88,** 7834–7838 (1991).
10. Watkins, J. C. & Evans, R. H. *Annu. Rev. Pharmacol. Toxicol.* **21,** 165–204 (1981).

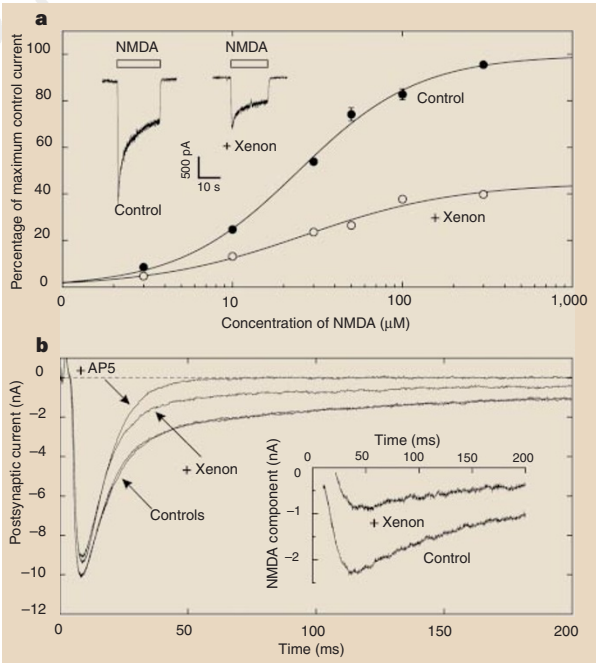

Figure 1 Xenon inhibits NMDA receptors in cultured rat hippocampal neurons. **a,** NMDA activates an inward current (in neurons clamped at − 60 mV) with an EC_{50} of 24 ± 2 μM NMDA and a Hill coefficient of 1.2 ± 0.1. Xenon inhibited the current by approximately 60% but did not significantly change either the EC_{50} or the Hill coefficient. Each data point represents the mean peak current from at least 6 cells. Inset, typical current traces (at 100 μM NMDA) in the presence and absence of xenon. **b,** Xenon selectively inhibits the NMDA-receptor-mediated component of glutamatergic excitatory postsynaptic currents (EPSCs). Neurons were voltage-clamped at − 60 mV; synaptic responses were stimulated by a 2-ms depolarizing pulse to + 20 mV. Control glutamatergic EPSCs displayed a characteristic biphasic decay. The slow component was completely blocked by 200 μM AP5, leaving the fast component almost unaffected. Inset, the NMDA-receptor-mediated component (the difference between the control EPSC and that in the presence of AP5) and its size in the presence of xenon (calculated by taking the difference between the EPSC in the presence of xenon and that in the presence of AP5). Control solutions were equilibrated at room temperature with 80% N_2 and 20% O_2, and test solutions with 80% Xe and 20% O_2.